Journal of Applied Mechanics and Technical Physics, Vol. 48, No. 3, pp. 346–360, 2007

SHOCK WAVES IN WATER WITH FREON-12 BUBBLES AND FORMATION OF GAS HYDRATES

V. E. Dontsov, V. E. Nakoryakov, and A. A. Chernov

UDC 532.529

The evolution of a shock wave and its reflection from a wall in a gas–liquid medium with dissolution and hydration are experimentally investigated. Dissolution and hydration behind the front of a moderate-amplitude shock wave are demonstrated to be caused by fragmentation of gas bubbles, resulting in a drastic increase in the area of the interphase surface and in a decrease in size of gas inclusions. The mechanisms of hydration behind the wave front are examined. Hydration behind the front of a shock wave with a stepwise profile is theoretically analyzed.

Key words: *shock wave, gas–liquid medium, fragmentation, dissolution, hydration.*

Power engineering companies that use natural gas as a source of energy face many important problems, including the efficiency of gas transportation and storage. If no pipeline is available, a promising method for gas transportation is its conversion to a gas-hydrate (solid) state and transportation at atmospheric pressure and reduced temperature (-10 to -20°C) [1–4]. According to the data of [1–4], the gas-hydrate technology of natural gas transportation and storage is particularly beneficial for small-scale and offshore fields of natural gas. Specialists' estimates predict that approximately 80% of the total world resources of free natural gas are located in medium- and small-scale deposits, and approximately half of them are located on the coastal shelf. Gas hydrates can be used on thermal power plants and in those industries that require large amounts of gas, where environmental pollution should be restricted.

There are various methods of intensification of gas hydration: fine-dispersion spraying of a jet saturated by a gas in a gas atmosphere [5–7], intense mixing of water saturated by a gas dissolved in it [6, 8], vibrational action on a liquid saturated by a gas [9], and ultrasonic action on a medium [10]. The main drawback of these methods is the low rate of gas hydration and, as a consequence, low efficiency of facilities developed on the basis of these methods. A possible application of this technology is desalination of mineral waters by the crystal-hydrate method. The use of Freon hydrates for this purpose is very simple in the engineering aspect and economically beneficial [11]. Experimental data on the rate of formation of Freon hydrates by intense mixing of salt water with a gas phase, aimed at water desalination, are described in [11].

The properties of gas hydrates, the basic laws, mechanisms of formation, and types of crystallization are described in [12–14]. Much attention is paid to physicochemical methods of investigating both artificial and natural gas hydrates.

Propagation of moderate-amplitude shock waves in a vertical shock tube filled by water with gas bubbles (Freon-12) with dissolution and hydration in the wave was experimentally investigated in the present work. Fragmentation of gas bubbles, their dissolution, and formation of the Freon-12 hydrate behind a moderate-amplitude shock wave in water with gas bubbles were studied. Hydration behind the front of a shock wave with a stepwise profile was theoretically analyzed, and the results were compared with experimental data.

The experiments were performed in a "shock tube" facility. The test section was a vertical thick-walled steel tube 1.5 m long with an inner diameter of 53 mm; the tube was bounded from below by a solid wall. The

Kutateladze Institute of Thermophysics, Siberian Division, Russian Academy of Sciences, Novosibirsk 630090; dontsov@itp.nsc.ru. Translated from Prikladnaya Mekhanika i Tekhnicheskaya Fizika, Vol. 48, No. 3, pp. 58–75, May–June, 2007. Original article submitted May 5, 2006; revision submitted August 17, 2006.

test section was filled by the liquid under vacuum conditions, which allowed avoiding origination of air bubbles in water. Gas bubbles of Freon-12 were injected through orifices 0.2 mm in diameter along the perimeter of the test section, in its bottom part. Such a method of bubble injection allowed us to obtain the liquid with a sufficiently high volume fraction of the gas. Depending on the volume fraction of the gas, the mean bubble radius was 2 to 3 mm. The working liquid was tap water saturated by Freon-12 to an equilibrium state corresponding to initial conditions (temperature and atmospheric pressure). The test section was thermostatted by pumping a cooling liquid between the outer wall and the test-section jacket. The outer surface of the jacket was covered by a heat insulator. A thermostat and a refrigerator were used for pumping the cooling liquid. The temperature of the liquid in the test section was measured by two thermocouples located in the top and bottom parts of the test section. The difference in temperature at the ends of the test section was smaller than 0.2°C. The mean initial volume fraction of the gas φ_0 averaged over the test-section length was calculated on the basis of changes in the height of the liquid column in the test section after injection of gas bubbles. The bubble size was determined by photographing by a digital camera with additional optical means through the optical windows in the top part of the test section. The resolution was 6.5 μm/pixel. Photographing of bubbles behind the shock wave involved a flash lamp triggered by a pulse generator at a prescribed time. Changing the delay of the triggering pulse made it possible to obtain photographs of bubbles in the liquid behind the shock-wave front with necessary time intervals. The flash duration was smaller than 1 μsec.

Stepwise pressure waves were generated by breakdown of a diaphragm separating the high-pressure chamber 2 m long and the test section. The diaphragm was cut by an air-operated knife at a prescribed time. The pressure-wave profiles were recorded by two piezo-electric pressure gauges (D1 and D2) and by a strain gauge flush-mounted with the inner wall along the test section. The strain gauge allowed us to measure the pressure profile at times of the order of 1 sec. The profile of the volume fraction of the gas behind the shock wave was measured by a conductivity gauge located in the middle of the test section. The gauge measured the volume fraction of the gas averaged over a volume that was the product of the cross-sectional area of the test section and a height of 20 mm. The reference time for averaging was determined by the time needed for the wave to pass through the gauge and amounted to less than 0.2 msec. The gauge signals were fed to an analog-to-digital converter and processed on a computer.

Hydration behind a stepwise shock-wave front was considered theoretically. We studied a volume of a saturated liquid with gas bubbles, which was subjected to shock-wave loading at the initial time. The pressure in the medium changed in a jump from P_0 to $P > P_0$. Let us consider a situation where such an action brings the medium to the range of phase states with possible hydration.

Like any other crystallization process, hydration includes fluctuating origination of crystallization centers (which is most probable on the free gas–water interface, i.e., on the bubble surface) and subsequent growth of the hydrate mass around the nuclei. New centers can appear both on the pure contact surface (homogeneous nucleation) and on admixture particles (heterogeneous nucleation). Simple estimates show that a typical time for nucleus origination $\tau_{\text{hom}} = 1/(J_{\text{hom}}\pi R_{\text{b}}^2) \approx 3.5$ min [12] in a homogeneous process on the bubble surface is much greater than the hydration time in the experiment: $\tau_{\text{h}}^{\text{exp}} = 1$–$10$ msec (R_{b} is the bubble radius and J_{hom} is the frequency of homogeneous nucleation). This allows us to conclude that nucleation in the process considered has a heterogeneous nature. In this case, nucleation of crystallization centers occurs extremely fast and can be considered as an instantaneous process.

The growth of the hydrate mass can be divided into two stages. At the first stage, after nucleation of crystallization centers, the surface-film hydrate intensely grows until it completely covers the free gas–water contact surface. The second stage is characterized by volume-diffuse formation of the hydrate, with the hydrate-forming agent diffusing through the hydrate film to water. If the radial growth rate of the hydrate film is constant (under unchanged thermodynamic parameters of the process), the volume-diffuse formation of the hydrate is exponentially slowed down with time (which is caused by film thickening). The rate of the volume-diffuse growth of the hydrate is several orders lower than the growth rate of the surface-film hydrate.

It was noted [14] that, in the case of formation of gas hydrates inside a gas bubble moving in water, the hydrate grows on the surface in the form of flakes, and the bubble walls remain flexible. Apparently, the "clothes" composed on hydrate crystals is not a significant obstacle for gas–water interaction, and there always exists a free contact surface, i.e., the volume-diffuse stage of growth of the hydrate mass is actually absent.

In view of the above-given reasoning, we assume that the hydration mechanism is as follows. The gas hydrate is formed on the bubble surface. Gas-hydrate nucleation occurs on heterogeneous centers and is assumed to be instantaneous. Gas-hydrate crystals have a spherical shape (in the first approximation), and their growth rate $v_{\rm h}$ is proportional to the degree of metastability of the medium, i.e., depends on overcooling with respect to the equilibrium state and is described by the relation $v_{\rm h} = K\Delta T$, where K is the kinetic coefficient and ΔT is the overcooling. This relation is valid for $t < (2\,{\rm Ku}\,\Delta T/T_{\rm eq})^{-1}a/(KT_{\rm eq})^2$, ${\rm Ku} = L/(cT_{\rm eq})$, when the latent heat of the phase transition, released owing to nucleus growth, can be neglected. Here $T_{\rm eq}$ is the equilibrium hydration temperature, a is the thermal diffusivity of the liquid, c is the heat capacity of the liquid, L is the hydration heat, and Ku is the Kutateladze criterion.

Obviously, the growth of the hydrate mass reduces the bubble size and, hence, the volume fraction of bubbles φ: $\varphi/\varphi_0 = V_{\rm b}/V_{\rm b0}$ ($V_{\rm b}$ is the volume of bubbles). We find $\varphi(t)$ using the following reasoning. The mass of the hydrate crystal growing on the surface of an individual bubble is

$$m_{\rm h} = \frac{4\pi}{3}\,\rho_{\rm h}\Big(\int\limits_0^t v_{\rm h}\,dt\Big)^3,$$

where $\rho_{\rm h}$ is the hydrate density. Hence, the total mass of all hydrate crystals $M_{\rm b}^{\rm h}$ on the bubble surface and the mass of the gas contained in the bubbles $M_{\rm b}^{\rm gh}$ are $M_{\rm b}^{\rm h} = 4\pi R_{\rm b0}^2 N_s m_{\rm h}$ and $M_{\rm b}^{\rm gh} = (\mu_{\rm g}/\mu_{\rm h})M_{\rm b}^{\rm h}$ (N_s is the surface density of active nuclei; $\mu_{\rm g}$ and $\mu_{\rm h}$ are the molar weights of the gas and hydrate, respectively).

To find the gas mass in the bubble $M_{\rm b}^{\rm g}$, we write the material balance relation $-dM_{\rm b}^{\rm g}/dt = dM_{\rm b}^{\rm gh}/dt$. This equation should be supplemented by the equation of state of the gas in the bubble $PV_{\rm b} = (M_{\rm b}^{\rm g}/\mu_{\rm g})RT$. This allows us to find the time evolution of the volume fraction of the gas

$$\frac{\varphi}{\varphi_0} = 1 - \frac{4\pi N_s \rho_{\rm h} RTK^3\Delta T^3 t^3}{PR_{\rm b0}\mu_{\rm h}}$$

and to determine the time $\tau_{\rm h}$ necessary for the entire gas contained in the bubbles to pass to the hydrate state:

$$\tau_{\rm h} = \frac{1}{K\Delta T}\Big(\frac{PR_{\rm b0}\mu_{\rm h}}{4\pi N_s\rho_{\rm h}RT}\Big)^{1/3}.$$

Note that the model described ignores collisions of grains of the gas-hydrate nuclei in the course of their growth. This occurs at the time t_* determined by the relation $v_{\rm h}t_* = (\pi N_s)^{-1/2}(\varphi(t_*)/\varphi_0)^{2/3}$. At $t > t_*$, obviously, the hydrate forms a continuous film on the bubble surface, and the total growth rate of the hydrate mass decreases. It is difficult to quantify the process at this stage because of a large number of random factors and problem parameters difficult to determine (in particular, it is difficult to take into account the bubble-boundary flexibility).

Fragmentation of Freon-12 gas bubbles in water behind a shock wave with a stepwise profile was examined experimentally. Figure 1 shows the photographs of the bubbles at the times t_f counted from the shock-wave arrival for different values of the dimensionless amplitude $\Delta P/P_0$ and a temperature $T = 16^\circ$C (P_0 is the initial pressure ahead of the shock wave). If the shock-wave amplitude is low ($\Delta P/P_0 \approx 0.3$), there are only cumulative jets formed inside the bubble, which leave the bubble through the rear (relative to the wave direction) surface of the bubble and deform the bubble boundary. As the wave amplitude increases ($\Delta P/P_0 \approx 0.6$), the cumulative jets entrain some part of the gas out of the original bubble and divide it into several fragments commensurable in size with the original bubble. Origination of cumulative jets behind shock waves in bubbles was observed in [15].

For $\Delta P/P_0 > 1$, the pattern of fragmentation of gas bubbles is qualitatively different. As was shown in [16], there arises instability of the gas–liquid interface owing to their relative motion (Kelvin–Helmholtz instability), which leads to fragmentation of the gas bubble into small gas inclusions ($\Delta P/P_0 \approx 1.3$). The size of inclusions is smaller than the original bubble size by an order of magnitude.

The Weber number ${\rm We} = 2R_{\rm b}\rho_{\rm g}V^2/\sigma$ for these parameters of the wave and the medium is close to the critical value, which confirms the development of the Kelvin–Helmholtz instability (V is the relative velocity of the gas bubble behind the shock wave, $\rho_{\rm g}$ is the gas density, and σ is the surface tension of the liquid). With a further increase in the wave amplitude, this instability leads to fragmentation of gas bubbles to even smaller fragments. Figure 1 shows the changes in geometry of the gas bubbles behind the leading front of the shock wave at $\Delta P/P_0 \approx 2.7$ at different times. At the leading front of the wave ($t_f = 0.3$ msec), there arise only cumulative jets in the bubbles, and the interface remains almost undeformed, while the interface becomes unstable behind the wave

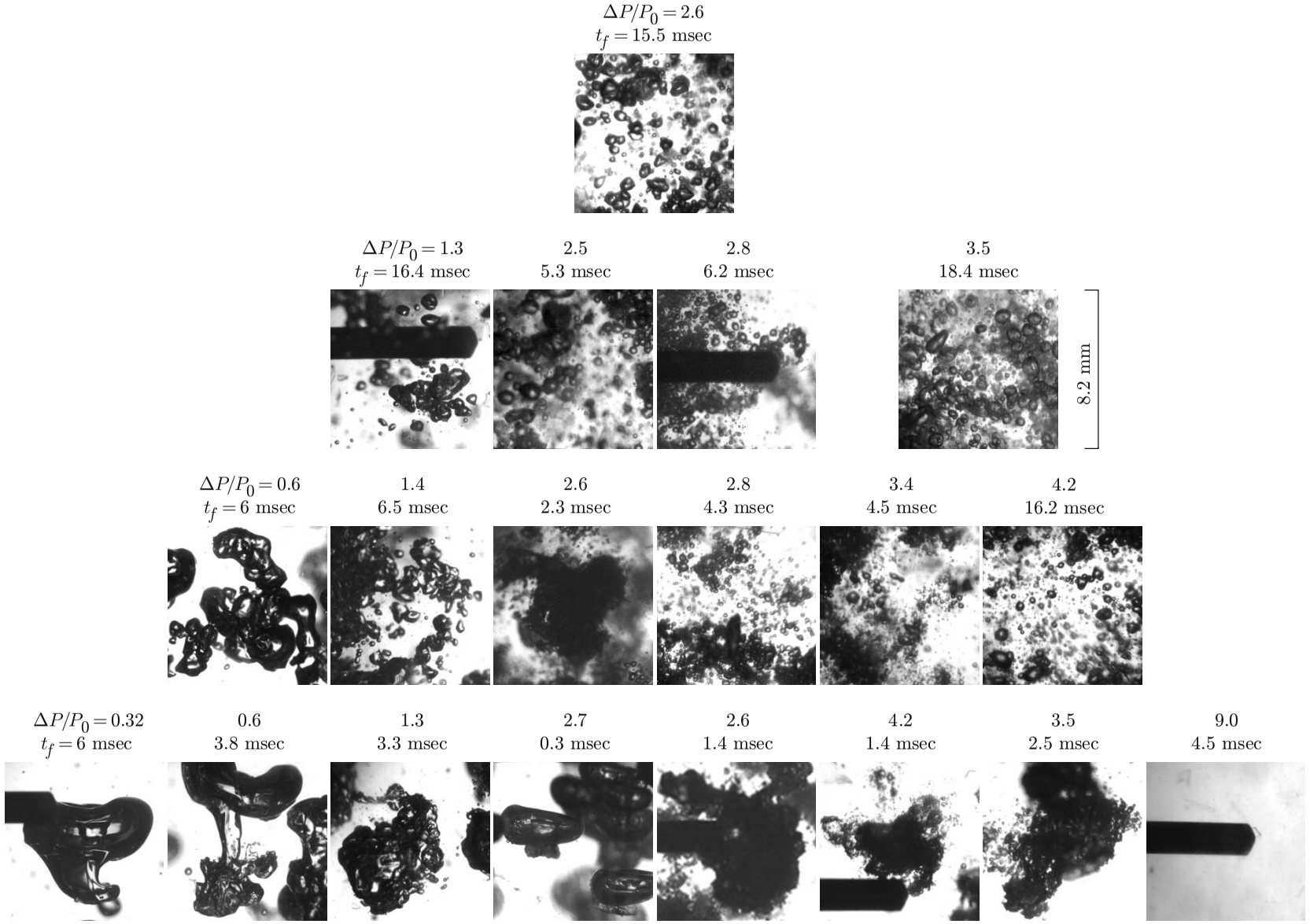

Fig. 1. Photographs of the bubbles behind the shock-wave front (T=16 °C)

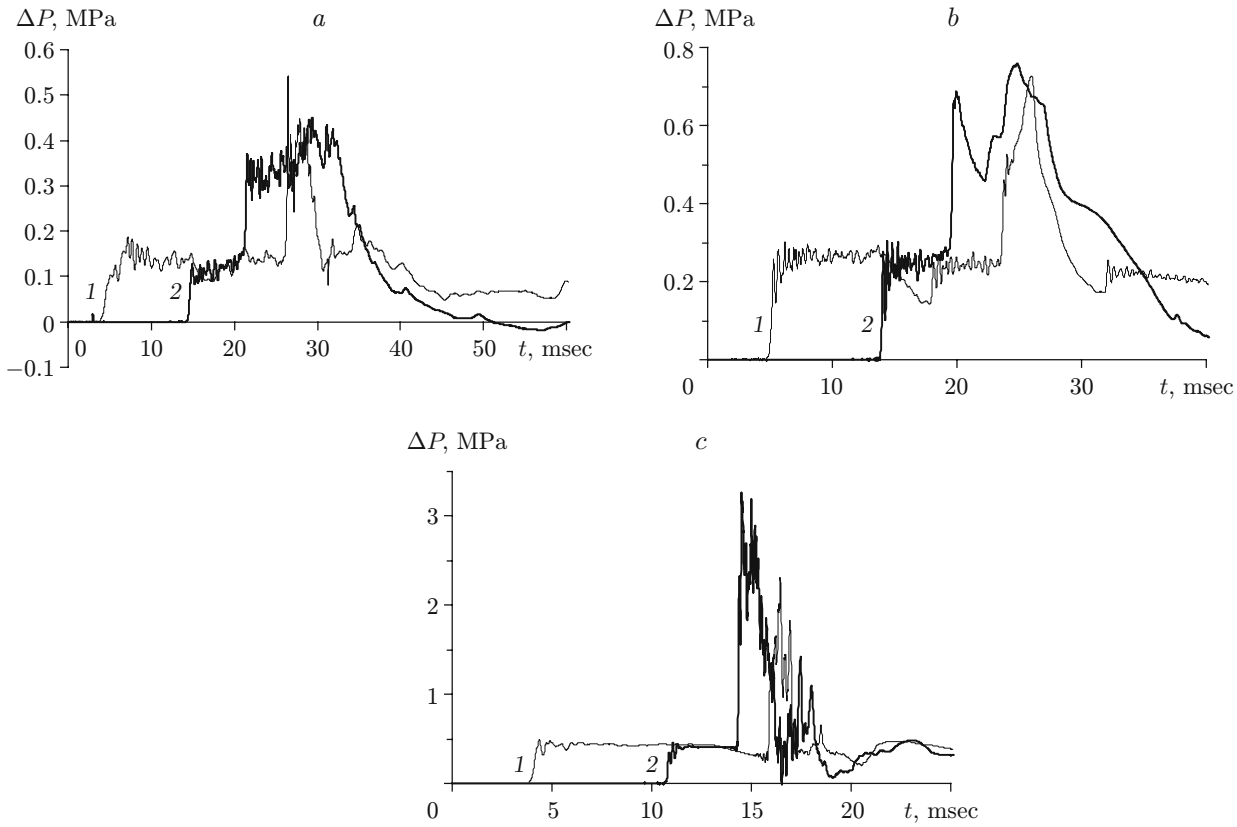

Fig. 2. Structure of the shock wave in water with Freon-12 bubbles ($T = 16°$C) for $\varphi_0 = 5.3$ (a), 6.4 (b), and 3.7% (c); curves 1 and 2 are obtained from the pressure gauges D1 and D2, respectively.

front ($t_f = 1.4$ msec), and small bubbles start to separate from the interface. After 4–5 msec, the bubbles behind the wave front are almost completely broken into individual fragments with a radius of 200–400 μm. In addition, the medium contains a large number of extremely small bubbles with a radius smaller than 100 μm. At high times behind the wave front ($t_f = 15.5$ msec), individual fragments of gas bubbles are fairly uniformly distributed in the liquid.

As the wave amplitude increases, fragmentation of gas bubbles becomes more intense, and a greater part of the gas occurs in bubbles of radius smaller than 100 μm ($\Delta P/P_0 = 3.5$–4.0). At the wave amplitude $\Delta P/P_0 \approx 10$, there occurs not only fragmentation of gas bubbles but also their complete dissolution behind the wave front during several milliseconds. The photograph only shows a rod 1.5 mm in diameter necessary for determining the photograph scale.

Let us consider propagation of a shock wave in a gas–liquid mixture and its reflection from a solid wall at $T = 16°$C. As this temperature is higher than the critical temperature of Freon-12 hydration ($T_{\text{cr}} = 12°$C), gas dissolution in the liquid is only possible. For amplitudes of the incident and reflected waves with no gas dissolution in the liquid, the amplitude of the reflected wave corresponds to the law of nonlinear reflection of a shock wave from a solid wall [17, 18] (Fig. 2a). With increasing wave amplitude, there begins gas dissolution in the liquid in the reflected wave, which distorts its profile (Fig. 2b). Owing to gas dissolution behind the front of the reflected shock wave, there arises a rarefaction wave, which reduces the amplitude of the leading front of the reflected wave. There is no dissolution in the incident wave, and there are no dispersion and dissipation effects on the wave structure. The velocity of the incident wave corresponds to the calculated adiabatic velocity of the shock wave [19, 20]. With a further increase in amplitude of the incident shock wave, the gas is almost completely dissolved at the front of the reflected wave, which is responsible for an increase in amplitude of the wave reflected from the solid wall (Fig. 2c). At the same time, an increase in the wave amplitude is accompanied by wave dissipation. As a result, the leading front of the incident shock wave gradually decays during wave propagation and, correspondingly, the wave velocity decreases.

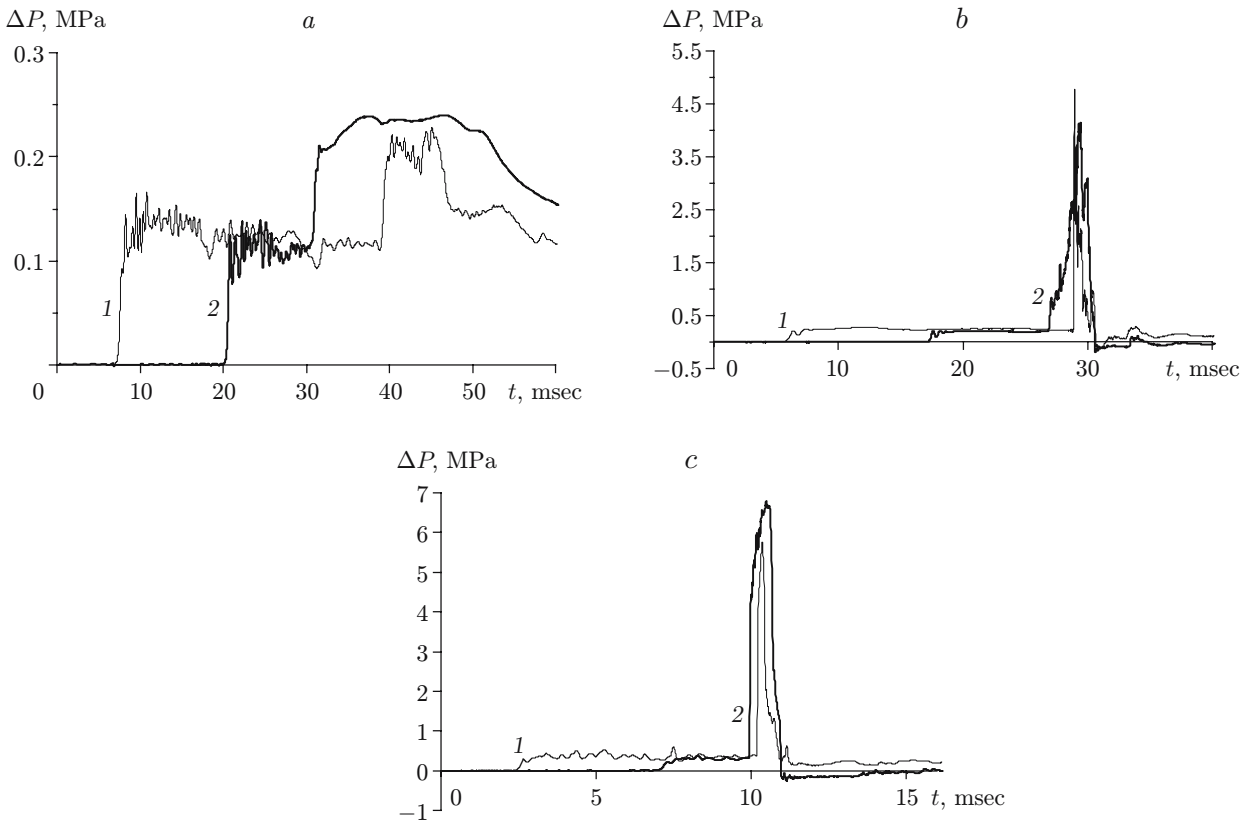

Fig. 3. Structure of the shock wave in water with Freon-12 bubbles ($T = 1°$C) for $\varphi_0 = 10.4$ (a), 8.9 (b), and 8.2% (c); curves 1 and 2 are obtained from the pressure gauges D1 and D2, respectively.

Now let us consider propagation of a shock wave in a gas–liquid mixture and its reflection from a solid wall at $T = 1°$C. This temperature is lower than the equilibrium temperature of formation of the Freon-12 gas hydrate at atmospheric pressure ($T_{\text{eq}} = 5°$C); hence, hydration in the shock wave is possible. As is demonstrated below, dissolution and hydration occur behind the reflected wave front already at a wave amplitude $\Delta P/P_0 \approx 1$, which leads to additional dissipation of the reflected wave. As a result, the amplitudes of the reflected waves are even lower than the amplitudes of the incident waves on both pressure gauges (Fig. 3a). With increasing wave amplitude, hydration in the incident wave begins, and the gas becomes completely hydrated at the front of the reflected wave (Fig. 3b). Hydration is seen to cause a more significant amplification of the reflected wave than dissolution (see Fig. 2b). The reason is that the rate of gas hydration behind the shock wave is much greater than the rate of gas dissolution in the liquid. With a further increase in the shock-wave amplitude, the gas is almost completely hydrated at the incident wave front, and the reflected wave propagates over the liquid containing gas-hydrate particles with a velocity of sound in the liquid (Fig. 3c). In this case, the law of shock-wave reflection corresponds to the law of reflection of a condensation wave from a solid wall in a vapor–liquid medium [17, 18]. Hydration behind the leading front of the incident shock wave does not affect its structure.

Figure 4 shows the experimental dependence of the shock-wave velocity in the liquid with gas bubbles U on the shock-wave amplitude for different values of the medium temperature. The curve shows the adiabatic shock-wave velocity calculated by the formula [19] $U/C = ((\gamma + 1)\Delta P/(2\gamma P_0) + 1)^{1/2}$, where C is the low-frequency adiabatic velocity of sound in the gas–liquid medium and γ is the ratio of specific heats. The experimental data for different temperatures of the medium almost coincide and agree with the calculated dependence. Hence, the process of gas dissolution and hydration in the liquid behind the shock wave in the examined range of wave and medium parameters exerts practically no effect on the velocity of the leading front of the wave. Deviation of experimental points from the calculated curve with increasing shock-wave amplitude is caused by the decay of the leading front of this wave. The shock-wave amplitude in the tests was found from the mean pressure behind the wave front, and

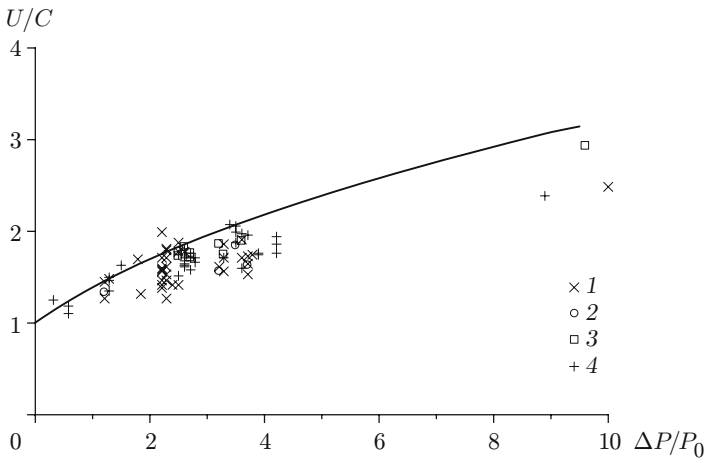

Fig. 4. Shock-wave velocity in water with Freon-12 bubbles versus the shock-wave amplitude for $T = 1$ (1), 4.9 (2), 6 (3), and 16°C (4).

the wave velocity was determined by the amplitude of the leading front of the wave, which is smaller than the mean pressure behind the wave front because of the wave decay.

To study gas dissolution and hydration behind the shock-wave front, we measured the profile of the local volume fraction of the gas behind the shock wave. Curve 1 in Fig. 5 shows the profile of the local volume fraction of the gas in the liquid at a temperature $T = 16$°C and different shock-wave amplitudes. As no gas hydrates are formed at this temperature, the volume fraction of the gas in the liquid behind the shock wave is determined only by gas compressibility and solubility. Figure 5a shows the profile of the local volume fraction of the gas in the liquid for a low wave amplitude, with the gas not dissolved behind the shock wave. The gas directly behind the front of the incident shock wave is compressed adiabatically, because the bubbles do not yet undergo fragmentation and the time of thermal relaxation of the gas in the bubbles is much greater than the leading front duration. As the bubbles undergo fragmentation, thermal relaxation occurs behind the wave front; the volume fraction of the gas decreases and approaches the values corresponding to isothermal compression of bubbles in the shock wave (curve 2). At the moment the front of the wave reflected from the solid bottom arrives, there is one more jumplike decrease in the volume fraction of the gas. As the bubbles are already fragmented at that time, the gas is compressed isothermally, and the volume fraction of the gas approaches the values corresponding to isothermal compression of bubbles in the reflected shock wave (curve 3). Behind the reflected wave, there arrives a rarefaction wave (see Fig. 2a), and the volume fraction of the gas recovers the previous value.

As the wave amplitude increases, fragmentation of bubbles in the shock wave proceeds faster, and the thermal relaxation reduces the time necessary to reach the volume fraction corresponding to isothermal compression (curve 2 in Fig. 5b). It is seen that there is no gas dissolution behind the incident wave, and the volume fraction remains constant until the reflected wave arrives. Behind the reflected wave front, the gas is isothermally compressed to values of φ corresponding to isothermal compression of bubbles in the reflected shock wave (curve 3), and then practically the entire amount of the gas becomes dissolved. Figure 5c shows the profiles of the volume fraction of the gas (curve 1) and the pressure recorded by the strain gauge (curve 4) at large times behind the wave front. In the rarefaction wave following the reflected wave, degasification of the liquid and expansion of the gas phase are observed. During the time $t = 1.5$–2.0 sec, the pressure in the medium decreases to the initial value P_0 (curve 4), and the volume fraction of the gas is not completely recovered (curve 1). Hence, some part of the gas (approximately 1/3) remains in the dissolved metastable state.

With a further increase in amplitude of the incident shock wave, the gas is isothermally compressed behind the leading front of the wave and becomes almost completely dissolved in the front of the reflected shock wave. As was demonstrated above (see Fig. 2c), this increases the amplitude of the wave reflected from the solid wall (Fig. 5d). In this case, no liquid degasification occurs after arrival of the rarefaction wave, and the gas remains in the metastable state during the entire observation period (2 sec). With a further increase in the shock-wave amplitude, complete dissolution of the gas behind the leading shock-wave front can be reached (Fig. 5e).

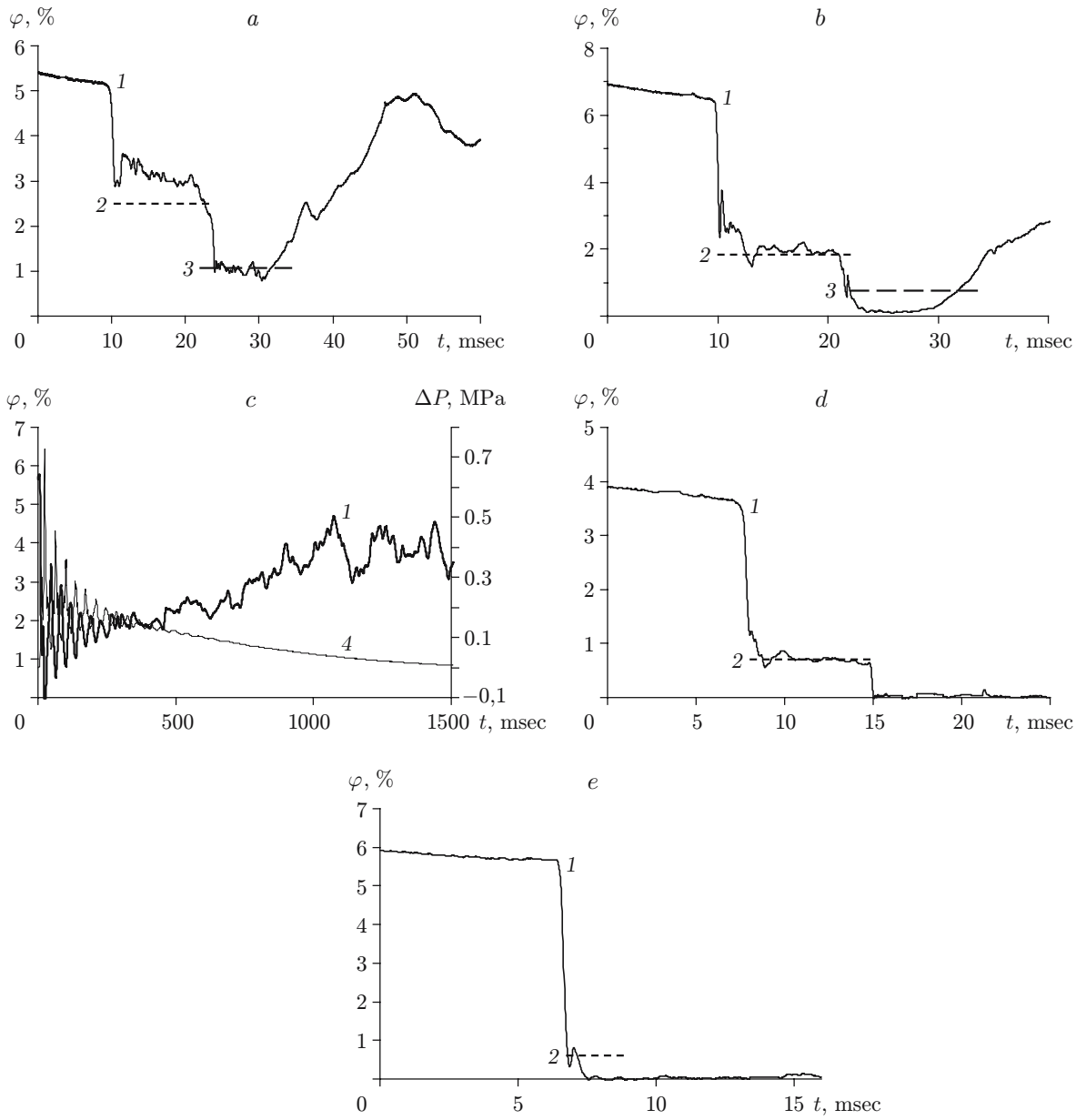

Fig. 5. Local volume fraction of the gas in water and pressure in the medium behind the front of a stepwise shock wave ($T = 16°$C): (a) $\Delta P/P_0 = 1.3$ and $\varphi_0 = 5.3\%$; (b) $\Delta P/P_0 = 2.5$ and $\varphi_0 = 6.4\%$; (c) $\Delta P/P_0 = 2.6$ and $\varphi_0 = 5.8\%$; (d) $\Delta P/P_0 = 4.2$ and $\varphi_0 = 3.7\%$; (e) $\Delta P/P_0 = 9$ and $\varphi_0 = 5.8\%$; the curves show the volume fraction of the gas (1), isothermal compression of bubbles in the incident shock wave (2), isothermal compression of bubbles in the reflected shock wave (3), and pressure in the medium (4).

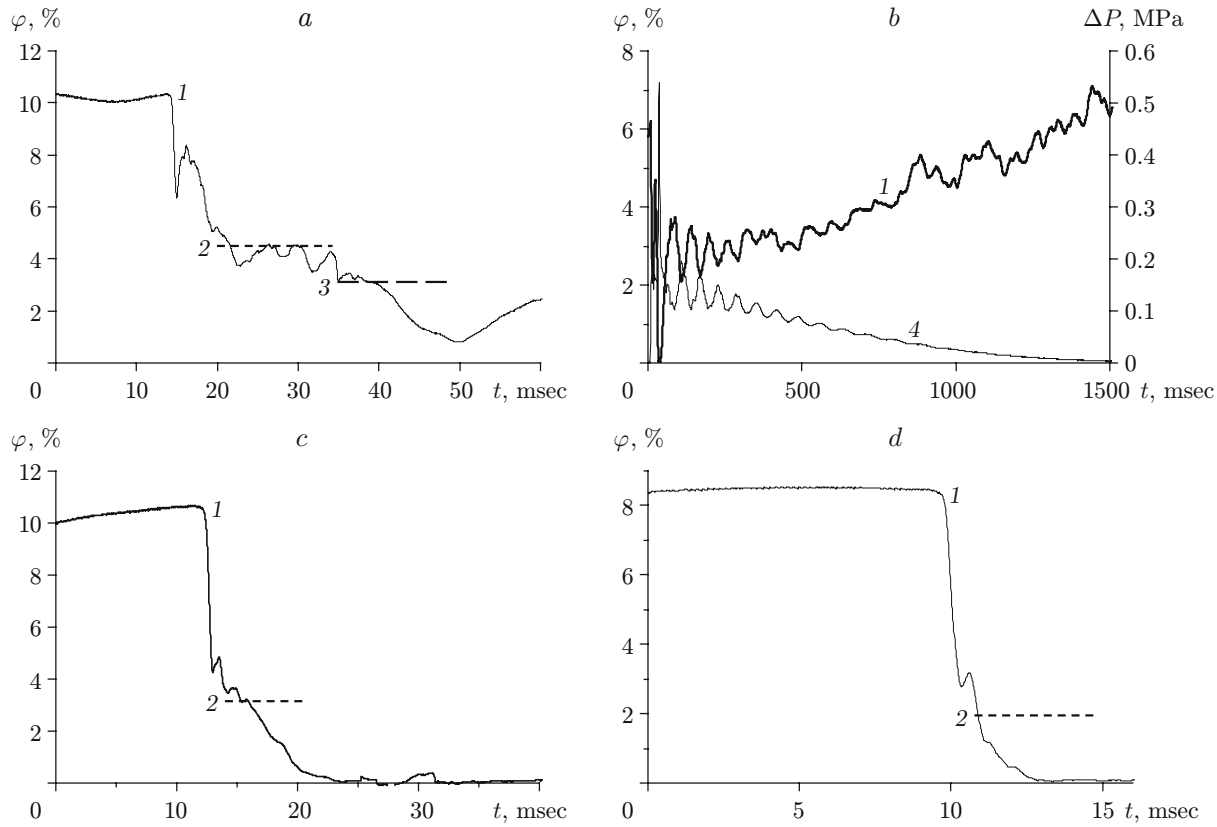

Fig. 6. Local volume fraction of the gas in water and pressure in the medium behind the front of a stepwise shock wave ($T = 1°$C): (a) $\Delta P/P_0 = 1.3$ and $\varphi_0 = 10.4\%$; (b) $\Delta P/P_0 = 1.8$ and $\varphi_0 = 6.2\%$; (c) $\Delta P/P_0 = 2.5$ and $\varphi_0 = 10.7\%$; (d) $\Delta P/P_0 = 3.3$ and $\varphi_0 = 8.4\%$; the curves show the volume fraction of the gas (1), isothermal compression of bubbles in the incident shock wave (2), isothermal compression of bubbles in the reflected shock wave (3), and pressure in the medium (4).

Let us consider hydration behind the shock-wave front. Note that the solubility of Freon-12 in water in the examined range of temperatures varies insignificantly and reaches approximately 2% per 1°C. Curve 1 in Fig. 6 shows the local volume fraction of the gas in the liquid at a temperature $T = 1°$C and different shock-wave amplitudes. The equilibrium pressure of formation of Freon-12 hydrates in water at $T = 1°$C is approximately 0.05 MPa. Hence, at $P_0 = 0.1$ MPa, the medium is in an overcooled (with respect to equilibrium) state, and overcooling is 4°C. Figure 6a shows the local volume fraction of the gas in the liquid for a low wave amplitude corresponding to the wave amplitude in Fig. 3a. As the bubbles undergo fragmentation behind the wave front owing to thermal relaxation, the volume fraction of the gas decreases to values corresponding to isothermal compression of bubbles in the shock wave (curve 2). At the moment the front of the wave reflected from the solid bottom arrives, there is one more jumplike decrease in the volume fraction of the gas corresponding to isothermal compression of bubbles in the reflected shock wave (curve 3), like in Fig. 5a. In contrast to Fig. 5a, however, the volume fraction of the gas in the reflected wave of an approximately identical amplitude is lower. This is caused by partial dissolution of the gas (as the solubility of Freon in water increases with decreasing temperature at a constant pressure) and its hydration. At low wave amplitudes, however, the process of gas hydration is metastable. After the rarefaction wave arrives at the measurement point, the volume fraction of the gas starts increasing and reaches the original value in 1–2 sec (curve 1 in Fig. 6b). Hence, the gas hydrate decomposes after the rarefaction wave arrival, and the subsequent gas parameters correspond to the ambient pressure.

Figures 6c and 6d show the local volume fractions of the gas for moderate amplitudes of the incident shock wave (curves 1). In contrast to the curves for the corresponding amplitudes in Figs. 5b and 5d, an intense decrease in the volume fraction is observed to start behind the leading front of the wave, which is caused by hydration. The

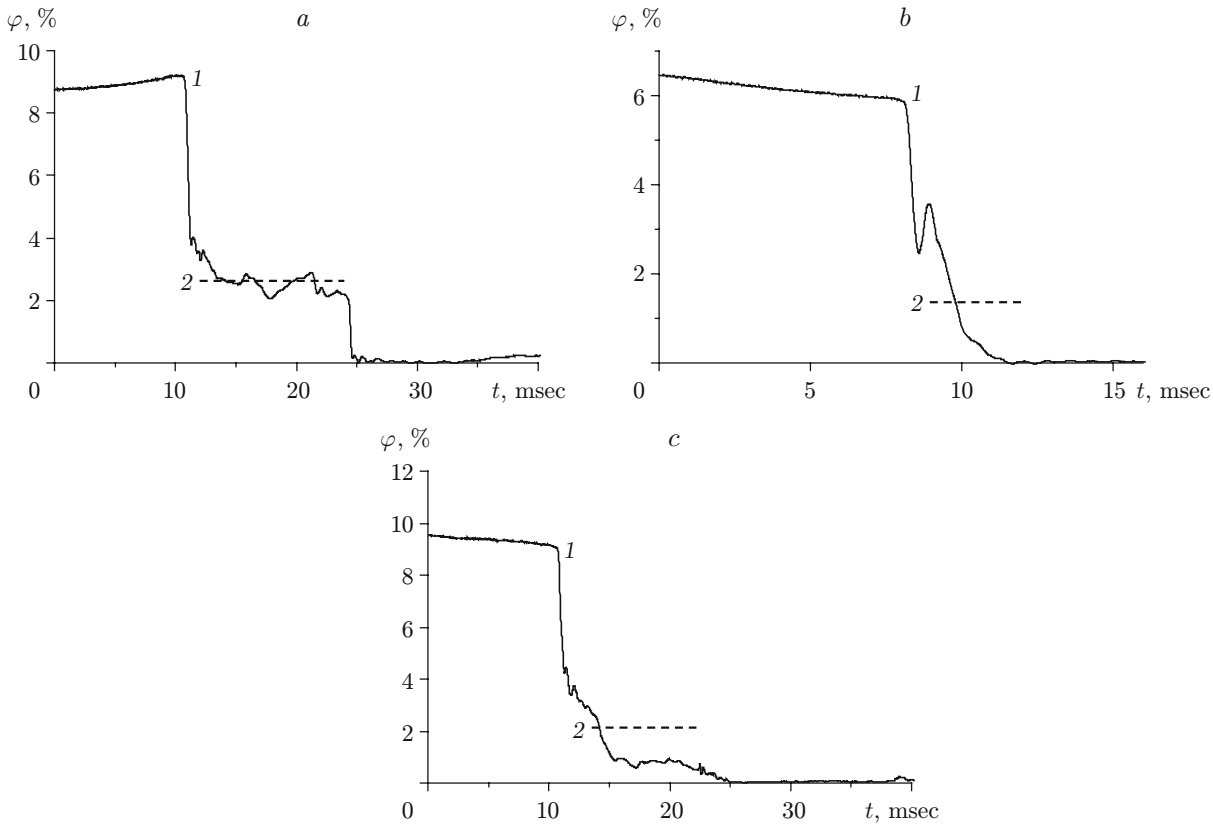

Fig. 7. Local volume fraction of the gas in water behind the front of a stepwise shock wave: (a) $T = 4.9°\text{C}$ $\Delta P/P_0 = 2.5$, and $\varphi_0 = 9.2\%$; (b) $T = 4.9°\text{C}$, $\Delta P/P_0 = 3.5$, and $\varphi_0 = 5.9\%$; (c) $T = 9.1°\text{C}$, $\Delta P/P_0 = 3.3$, and $\varphi_0 = 9.1\%$; curves 1 and 2 show the volume fraction of the gas and isothermal compression of bubbles in the shock wave.

characteristic time of complete hydration of the gas behind the shock wave is several milliseconds, and the growth rate of the gas hydrate is several orders higher than the rate of the volume-diffuse growth of gas hydrates obtained in [11–14]. Thus, we can assume that the adsorption growth of the hydrate film on the gas-bubble surface, which is determined by kinetic parameters and is characterized by a high rate, leads to complete conversion of the gas contained in the bubbles to the hydrate film or to disintegration of the hydrate film. A new hydrate film is then formed on the gas–liquid interface, and the gas hydrate is formed with the volume-diffuse stage of growth being skipped. Formation of the hydrate film on the bubble surface in the form of flakes is also possible. In this case, the hydrate film does not prevent the liquid and solid phases from approaching the interface, which favors the formation of a new hydrate film.

As the wave amplitude increases, the time needed for the gas to pass to the hydrate state behind the wave front decreases. If the wave amplitude is sufficiently high ($\Delta P/P_0 \approx 10$), the time of gas hydration behind the shock wave becomes commensurable with the time of fragmentation of gas bubbles. In this case, the hydration process, like to dissolution process (see Fig. 5e), is determined by the time of fragmentation of the gas phase behind the shock-wave front.

We study the effect of the medium temperature on the hydration process. Figures 7a and 7b show the local volume fractions of the gas in the liquid for different wave amplitudes and a temperature $T = 4.9°\text{C}$. This temperature is close to the equilibrium temperature of hydration at atmospheric pressure ($T_{\text{eq}} = 5°\text{C}$ at $P_0 = 0.1$ MPa). Figure 7a shows the volume fraction of the gas behind the shock wave with an amplitude $\Delta P/P_0 = 2.5$ (curve 1). By comparing it with the volume fraction of the gas in Fig. 6c, we see that an increase in temperature with a constant wave amplitude interrupts the hydration process behind the incident shock wave at the examined times. Thus, in the course of gas hydration, the degree of overcooling behind the shock wave relative to the equilibrium

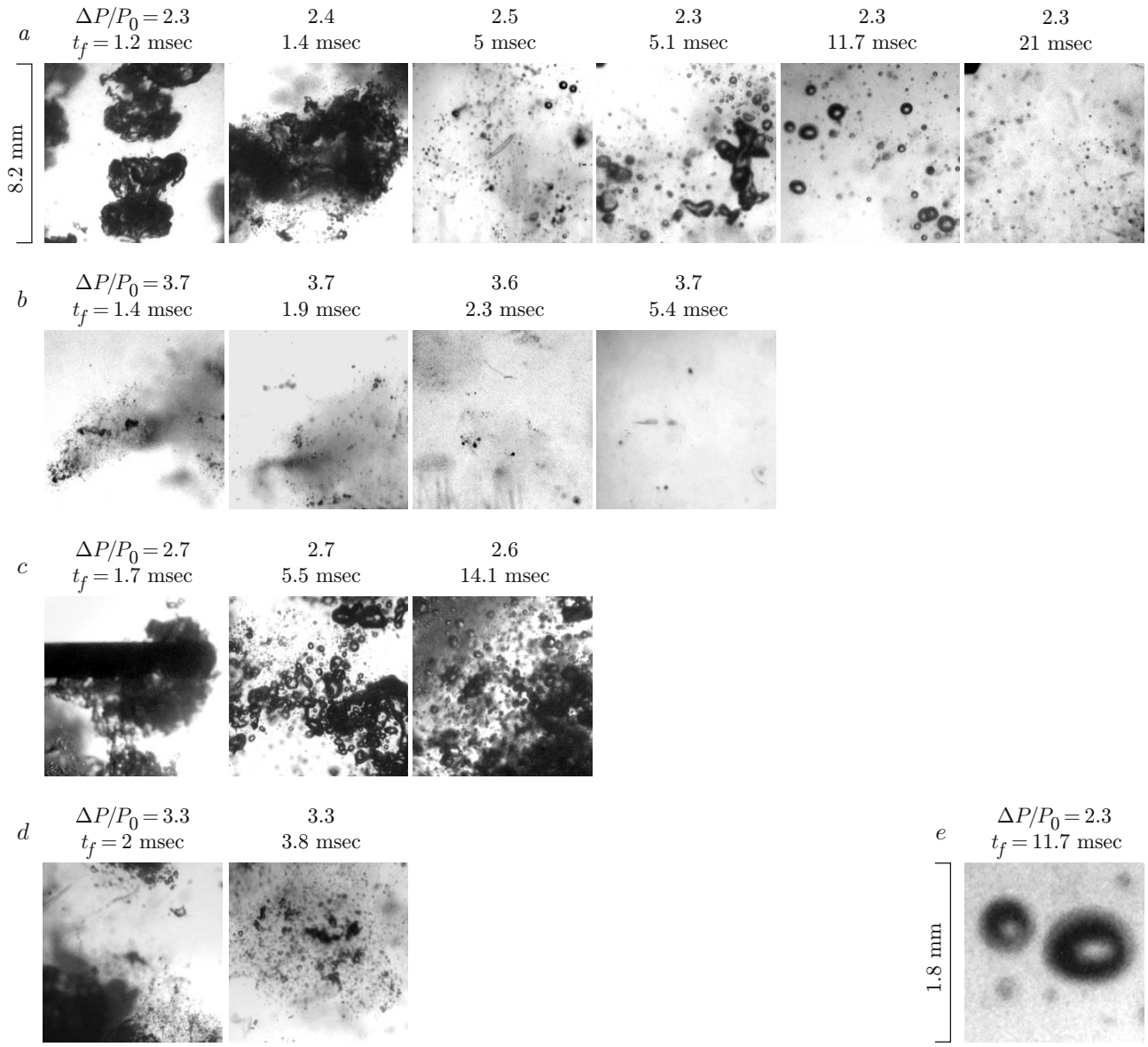

Fig. 8. Photographs of the bubbles behind the shock-wave front for $T = 1$ (a, b, and e) and 6°C (c and d).

state is a governing parameter. As the shock-wave amplitude increases, hydration in the incident shock wave starts, but the rate of this process is lower than that at a temperature $T = 1$°C (Fig. 7b). Figure 7c shows the volume fraction of the gas behind the shock wave with an amplitude $\Delta P/P_0 = 3.3$ at $T = 9.1$°C (curve 1). By comparing the volume fractions of the gas in Figs. 6d and 7b, we can conclude that a further increase in temperature leads to a more significant decrease in the hydration rate. For the shock-wave amplitude used, the gas does not have enough time to completely pass to the gas-hydrate state before the reflected wave arrives.

As the temperature of the medium increases to $T = 11$°C, the hydration process behind the shock wave ceases because it is impossible to reach a necessary level of metastability behind the shock-wave front ($T_{\text{cr}} = 12$°C is the critical temperature for formation of the gas hydrate of Freon-12).

Let us consider the behavior of the gas bubbles behind the shock-wave front at a temperature $T = 1$°C and different wave amplitudes (Figs. 8a and 8b). At $t_f = 1$–2 msec and $\Delta P/P_0 \approx 2.4$, the bubbles are compressed and undergo fragmentation (as at $T = 16$°C) without hydration (Fig. 8a). With increasing time t_f, hydration begins, which leads to a drastic decrease in the content of the gas phase in the liquid ($t_f \approx 5$ msec). A comparison of the

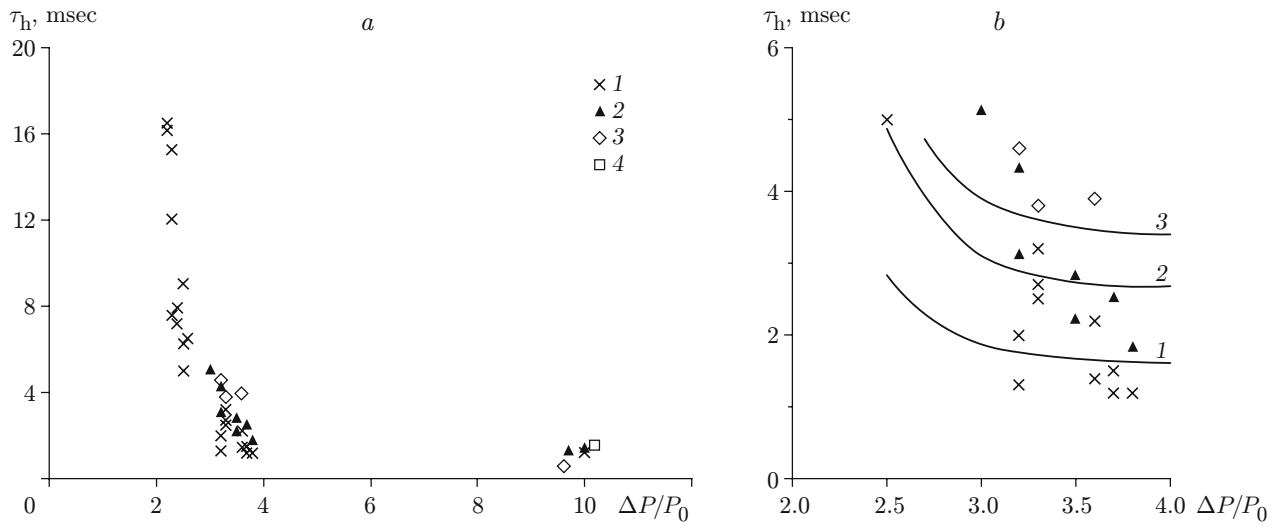

Fig. 9. Time of gas hydration behind the front of a stepwise shock wave versus the wave amplitude: the points and curves refer to the experimental and calculated data for $T = 1$ (1), 4.9 (2), 6 (3), and 9.1°C (4).

bubble photographs at $t_f \approx 5$ msec shows that the hydration rate is strongly affected even by small changes in the wave amplitude. At $t_f > 10$ msec, only individual gas bubbles are observed, while the major part of the gas has already passed to the gas-hydrate state, which is consistent with the behavior of the local volume fraction of the gas (see Fig. 6c). The resolution of the optical system allow us to distinguish bubbles of radius greater than 10–20 μm; hence, individual gas-hydrate particles cannot be identified in the photographs presented. Bubbles of radius of 200–300 μm, however, in the course of hydration display lighter bandelets on the background of the black boundary of the gas bubbles. Figure 8e shows two bubbles in an enlarged scale. One can clearly see semitransparent bandelets near the bubble boundaries, which apparently consist of individual gas-hydrate particles.

Figure 8b shows the photographs of the bubbles in the liquid at $\Delta P/P_0 \approx 3.7$. Already at $t_f = 1.4$–1.9 msec, the gas bubble is almost completely fragmented and hydrated, which is consistent with the behavior of the local volume fraction of the gas (see Fig. 6d). Only small individual bubbles and gas-hydrate particles are visible at the place where the bubbles were located prior to fragmentation. At high times ($t_f = 5.4$ msec), one can only see a gray background, which is caused by the presence of gas-hydrate particles.

Figures 8c and 8d show the photographs of the bubbles behind the front of the waves with amplitudes $\Delta P/P_0 \approx 2.7$ and 3.3, respectively, at $T = 6$°C. The behavior of gas bubbles in Fig. 8c corresponds to the behavior of gas bubbles behind the wave of the same amplitude in the medium without hydration (see Fig. 1). Such a behavior of the gas phase also corresponds to the profile of the volume fraction of the gas in Fig. 7a, where no gas hydration behind the incident shock wave is observed. As the wave amplitude increases, hydration does occur behind the shock-wave front (Fig. 8d), but its intensity is significantly lower than that at $T = 1$°C. The reason is the decrease in the degree of overcooling with increasing temperature of the medium with respect to the equilibrium state behind the shock wave.

Figure 9 shows the experimental dependence of the time of gas hydration τ_h behind the shock-wave front on the wave amplitude and the results calculated by the proposed model for different medium temperatures. The gas-hydration time in the experiments was determined from the leading front of the wave to the level $0.1\varphi_1$ [$\varphi_1 = (P_0/P_1)\varphi_0$ is the calculated volume fraction of the gas behind the shock-wave front with isothermal compression of bubbles, φ_0 is the initial volume fraction of the gas, and $P_1 = P_0 + \Delta P$ is the pressure behind the shock-wave front]. The hydration time decreases with increasing shock-wave amplitude, owing to fragmentation of gas bubbles and an increase in pressure behind the shock-wave front. Fragmentation of bubbles leads to a drastic decrease in size of gas inclusions and to an increase in the interphase surface area, while an increase in pressure behind the wave front enhances overcooling with respect to the equilibrium state behind the shock wave and, correspondingly, the level of metastability. It is seen in Fig. 9 that formation of gas hydrates starts at a certain minimum wave

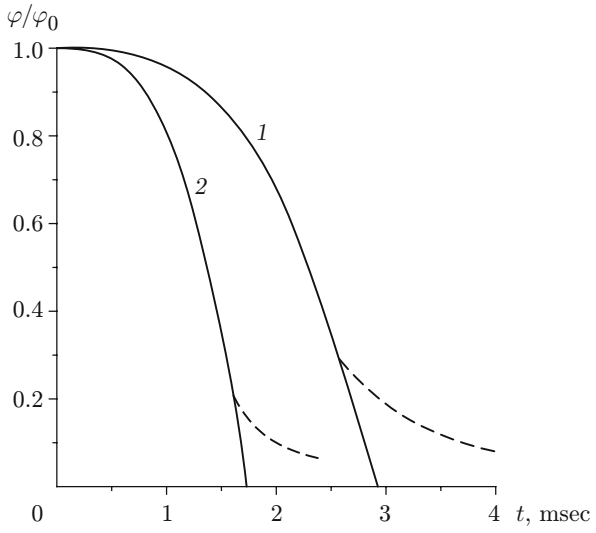

Fig. 10

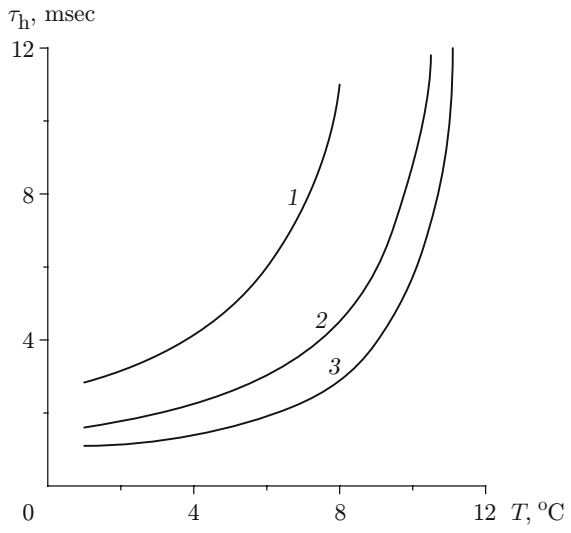

Fig. 11

Fig. 10. Calculated profiles of the dimensionless volume fraction of the gas in the course of hydration behind the shock-wave front ($T = 1°$C): 1) $\Delta P/P_0 = 2.5$ and $R_\text{b} = 400$ μm; 2) $\Delta P/P_0 = 3.3$ and $R_\text{b} = 100$ μm; the solid curves are calculated with collisions of gas-hydrate grains at the gas-bubble edge being ignored; the dashed curves show the qualitative dependence $\varphi/\varphi_0(t)$ for complete overlapping of the gas hydrate with the bubble surface.

Fig. 11. Calculated time of gas hydration behind the shock-wave front versus the medium temperature: 1) $\Delta P/P_0 = 2.5$ and $R_\text{b} = 400$ μm; 2) $\Delta P/P_0 = 3.3$ and $R_\text{b} = 100$ μm; 3) $\Delta P/P_0 = 10$ and $R_\text{b} = 10$ μm.

amplitude. At a temperature $T = 1°$C, the threshold value of the shock-wave amplitude is $\Delta P/P_0 \approx 2$, which is close to the threshold value of the wave amplitude responsible for fragmentation of gas bubbles into small gas inclusions (see Fig. 1). An increase in temperature increases the minimum value of the wave amplitude at which hydration occurs. At a temperature $T = 4.9°$C and shock-wave amplitude $\Delta P/P_0 \approx 2.5$, hydration behind the front of the incident shock wave does not occur at the examined times, and the threshold value of the shock-wave amplitude is within $\Delta P/P_0 = 2.5$–3.0. At $T = 9.1°$C and $\Delta P/P_0 \approx 3.5$, gas hydrates are formed behind the front of the incident shock wave, but there is not enough time even for 90% of the gas to get hydrated. At high wave amplitudes ($\Delta P/P_0 \approx 10$), with a rather high degree of metastability, the gas-hydration time is mainly determined by the time of fragmentation of gas bubbles behind the wave front.

The results on Freon-12 hydration calculated by the proposed model are described below. The calculations were performed at temperatures $T = 1$, 4.9, and 6°C and initial pressure $P_0 = 0.1$ MPa. The bubble radius varied depending on $\Delta P/P_0$ in accordance with test conditions imposed (from 400 μm at $\Delta P/P_0 \approx 2.5$ to 100 μm at $\Delta P/P_0 \approx 4$). As there are no necessary data on the kinetic coefficient of hydration K available in the literature, we used the value of the kinetic coefficient of water crystallization $K = 10^{-3}$ m/(sec · K). The number of nucleation centers was assumed to be equal to the mean number of admixture particles in tap water: $N_s = 10^8$ m^{-2}.

Figure 9b shows the calculated and experimental dependences of the hydration time τ_h on the shock-wave amplitude. Even a rather simplified model offers an adequate description of the main laws of hydration behind the shock wave. The calculations confirm that the decrease in hydration time with increasing $\Delta P/P_0$ is mainly caused by the decrease in the characteristic size of gas inclusions behind the shock wave owing to fragmentation of gas bubbles, while the increase in hydration time with increasing temperature is caused by the decrease in the degree of overcooling inherent in the process.

Figure 10 shows the calculated profiles of the dimensionless volume fraction of the gas in the course of hydration behind the shock-wave front for different parameters of the wave and the medium. As was demonstrated above, the model allows only determining the moment of collision of individually growing grains of the gas hydrate. It does not seem possible to quantify the process at $t > t_*$. Nevertheless, the calculated curves are in qualitative

agreement with the experimental profiles of the volume fraction of the gas behind the shock-wave front in Figs. 6c and 6d. It should be noted that the moment of collision of gas-hydrate grains on the bubble surface t_* for large bubble radii occurs earlier at high volume fractions than at lower volume fractions. For this reason, large bubbles in the experiments are hydrated slower than it is predicted by calculations, which is really observed for low values of $\Delta P/P_0$ (see Fig. 9b).

Figure 11 shows the calculated dependences of the time of gas hydration behind the shock-wave front on the medium temperature for different parameters of the wave and the medium. As the temperature increases, the degree of overcooling decreases, which increases the gas-hydration time. For lower wave amplitudes (curve 1), the overcooling is smaller; hence, the hydration time is greater for this temperature of the medium. As the critical temperature of Freon-12 hydration is approached ($T_{\text{cr}} = 12^\circ$C), the hydration time substantially increases, which is also caused by the decrease in overcooling (metastability) of the medium. At $T \approx 11^\circ$C, the process of hydration behind the shock wave of any amplitude almost ceases, which agrees with experimental data.

Thus, the process of fragmentation of gas bubbles behind a moderate-amplitude shock wave in a gas–liquid medium is studied experimentally. The threshold value of the wave amplitude corresponding to the transition from jet fragmentation to fragmentation due to instability of the interphase boundary for Freon-12 bubbles in water is obtained.

The evolution of the shock wave, its structure, and its reflection from a solid wall in a gas–liquid medium with dissolution and hydration are examined in experiments. It is demonstrated that these processes can lead to either dissipation of the reflected wave or to its amplification.

The processes of dissolution and hydration behind a moderate-amplitude shock wave are studied. These processes are shown to be caused by fragmentation of gas bubbles, leading to a drastic increase in the interphase surface area and to a decrease in size of gas inclusions. The characteristic time of complete hydration of the gas behind the shock wave is found to be several orders smaller than that obtained by other methods of hydration and to reach several milliseconds. Mechanisms of hydration behind the wave front are examined. Hydration is shown to occur owing to adsorption growth of the hydrate film on the gas-bubble surface, which is determined by kinetic parameters (overcooling and pressure in the medium) and is characterized by an extremely high rate.

Hydration behind a stepwise shock wave is theoretically analyzed, and comparisons with experimental data are performed.

This work was supported by the Russian Foundation for Basic Research (Grant No. 06-01-00142) and by the Program No. 4.13.8 of the Department of Power Engineering, Mechanical Engineering, Mechanics, and Control Processes of the Russian Academy of Sciences.

REFERENCES

1. T. Takaoki, T. Iwasaki, Y. Katoh, et al., "Use of hydrate pellets for transportation of natural gas. 1. Advantage of pellet form of natural gas hydrate in sea transportation," in: *Proc. of the 4th Int. Conf. on Gas Hydrates* (Yakohama, Japan, May 19–23, 2002), S. n., Yakohama (2002), pp. 982–986.
2. Y. Nakajima, T. Takaoki, K. Ohgaki, and S. Ota, "Use of hydrate pellets for transportation of natural gas. 2. Proposition of natural gas transportation in form hydrate pellets," *ibid.* pp. 987–990.
3. S. Ota, H. Uetani, and Y. Kawano, "Use of hydrate pellets for transportation of natural gas. 3. Safety measures and conceptual design of natural gas hydrate pellet carrier," *ibid.*, pp. 991–996.
4. J. Gudmundsson, M. Mork, and O. Graff, "Hydrate non-pipeline technology," *ibid.*, pp. 997–1002.
5. R. Ohmura, S. Kashiwazaki, S. Shiota, et al., "Structure-1 and structure-2 hydrate formation using water spraying," *ibid.*, pp. 1049–1054.
6. K. Miyata, T. Okui, H. Hirayama, et al., "A challenge to high-rate industrial production of methane hydrate," *ibid.*, pp. 1031–1035.
7. I. S. Gudmundsson, "Method for obtaining gas hydrates for transportation and storage," RF Patent 2200727, C 07 C 5/02, No. 97112086/06, Appl. 07.02.1997, Publ. 03.20.2003, Bul. No. 8.
8. V. S. Yakushev, "Method of extraction and transportation of natural gas from gas and gas-hydrate sea-based deposits, called flowers and bees," RF Patent 2198285, E 21 B 43/01, No. 98113838/03, Appl. 07.13.1998, Publ. 02.10.2003, Bul. No. 4.

9. K. B. Komissarov and V. A. Finochenko, "Facility for obtaining gas hydrates," RF Patent 2045718, F 25 D 3/12, No. 5044706/13, Appl. 05.29.1992, Publ. 10.10.1995, Bul. No. 28.
10. Y. Kozo, F. Tetsuro, K. Takahiro, and K. Yuichi, GB Patent 2347938 A, C 07 C7/152, No. 0006039.2, Publ. 09.20.2000.
11. L. F. Smirnov, "Experimental study of Freon-12 hydration," *Kholod. Tekh.*, No. 2, 28–34 (1973).
12. Y. F. Makogon, *Gas Hydrates, Preventing Their Formation, and Their Applications* [in Russian], Nedra, Moscow (1985).
13. Y. F. Makogon, *Hydrates of Hydrocarbons*, Pennwell, Tulsa (Oklahoma) (1997).
14. V. A. Istomin and V. S. Yakushev, *Gas Hydrates in Nature* [in Russian], Nedra, Moscow (1992).
15. V. K. Kedrinskii and R. I. Soloukhin, "Compression of a spherical gas cavity in water by a shock wave," *Prikl. Mekh. Tekh. Fiz.*, No. 1, 27–29 (1961).
16. B. E. Gel'fand, S. A. Gubin, S. M. Kogarko, et al., "Destruction of gas bubbles in a liquid by shock waves," *Izv. Akad. Nauk SSSR, Mekh. Zhidk. Gaza*, No. 4, 51–56 (1975).
17. R. I. Nigmatulin, *Dynamics of Multiphase Media*, Part 1, Hemisphere Publ., New York (1991).
18. V. E. Dontsov and B. G. Pokusaev, "Shock waves and mass transfer behind the shock wave in bubbly media," *Teoret. Osn. Khim. Tekhnol.*, **33**, No. 5, 485–494 (1999).
19. V. E. Nakoryakov, B. G. Pokusaev, and I. R. Shreiber, *Wave Dynamics of Gas–Liquid and Vapor–Liquid Media* [in Russian], Énergoatomizdat, Moscow (1990).
20. G. M. Lyakhov, *Waves in Soils and Porous Multispecies Media* [in Russian], Nauka, Moscow (1982).